Novel Target Designs to Mitigate Hydrodynamic Instabilities Growth in Inertial Confinement Fusion

Xiumei Qiao[1] and Ke Lan[1,2,*]

[1]Institute of Applied Physics and Computational Mathematics, Beijing 100094, China

[2]HEDPS, Center for Applied Physics and Technology, and College of Engineering, Peking University, Beijing 100871, China

(Received 17 December 2020; revised 4 March 2021; accepted 15 April 2021; published 4 May 2021)

High density carbon (HDC) ablator is one of the promising candidates toward thermonuclear ignition in inertial confinement fusion (ICF), but it shows the largest ablation front instability growth as compared to other traditional ablator materials. In this Letter, we propose a novel HDC-CH capsule design, opening the way to mitigate the hydrodynamic instabilities by using CH as the outermost ablator layer, while keeping HDC as the main ablator for maintaining the advantage of short laser pulses. The CH layer is completely ablated during the shock transit phase. In the HDC-CH design, it is the first shock reflected from the HDC/CH interface that meets the ablation front first, which reduces the ablation front growth factor by about one order of magnitude at peak implosion velocity due to the Richtmyer-Meshkov and the Rayleigh-Taylor instabilities. Our 2D simulation studies demonstrate convincingly that the ablation front growth factor of the HDC-CH capsule can be significantly reduced at both the end of shock transit phase and the time at peak implosion velocity, as compared to a HDC capsule. This novel HDC-CH capsule not only keeps the main advantage of the HDC ablator, but also has the advantage of low hydrodynamic instabilities, which can provide a larger margin toward ICF ignition. It can be applicable to both indirect-drive and direct-drive targets.

DOI: 10.1103/PhysRevLett.126.185001

The most important goal of inertial confinement fusion (ICF) is to achieve ignition, which is the major step on the path to controlled fusion energy. This problem has been quested by scientists worldwide for over a half century [1–3]. In indirect-drive ICF, a spherical capsule contains deuterium tritium (DT) fusion fuel inside an ablator shell, and the ablator shell is quickly heated and ablated by x rays and compresses the DT fuel to ignition condition via rocket motion. Latest ICF experiments at the National Ignition Facility (NIF) [4–6] in the United States have reached major milestones [7–10], such as the so-called alpha-heating regime, in which the self-heating by fusion products becomes dominant, with neutron yields exceeding 2×10^{16}. However, the fusion yield on the NIF still remains significantly lower than predicted by simulations. The two important obstacles preventing ignition are laser plasma instabilities (LPI) and hydrodynamic instabilities (HI), which are both strongly conditioned by the choice of ablator material.

Several ablators are explored for a capsule design in the indirect-drive ICF [11–13], and two of the best candidates are the glow discharge polymer plastic (CH) and high density carbon (HDC) [14]. The CH ablator is easy to make and it is mainly used in the National Ignition Campaign on the NIF [15], but it is hard to simultaneously achieve a high fuel compression with an effective HI suppression. In contrast, the HDC ablator has the advantage of high density, allowing us to use thinner capsules and shorter laser pulses thus leading to a low level of LPI and a better symmetry control in the low gas filled hohlraums [16,17]. As a result, the HDC capsule has become one of the promising candidates toward ignition [10,18], achieving the best implosion performance on the NIF with fusion energies up to 55 kJ [9]. Nevertheless, the development of HI in HDC capsule is more severe than in the CH capsules [19–21], which is adverse in achieving the yield expected in the ideal case of spherical symmetry.

In this Letter, we propose a novel HDC-CH capsule design to mitigate the hydrodynamic instabilities by using CH as the outermost ablator layer while keeping HDC as the main ablator for maintaining its advantage of short laser pulses. The CH layer in HDC-CH capsule is completely ablated during the shock transit phase, and its role is to use the interface between lower density CH and higher density HDC to mitigate the ablation front instability growth during the shock transit phase. From our 2D simulation studies, compared with a HDC capsule, the ablation front growth factor of the HDC-CH capsule can be significantly reduced during both shock transit phase and acceleration phase. This novel design is applicable to a broader design space, not only to indirect-drive, but also direct-drive targets. In this Letter, we focus on the indirect-drive approach.

Presented in Fig. 1 is the schematics of the HDC-CH capsule and a HDC capsule for comparison, together with their corresponding radiation drives. According to our designs, the two capsules have similar yields expected in

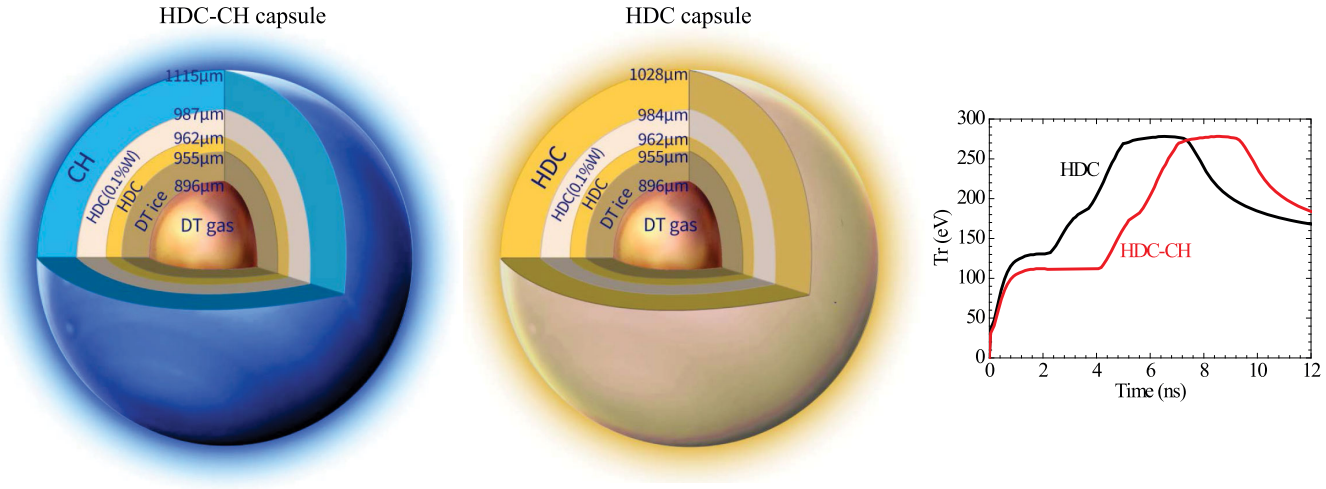

FIG. 1. Schematics of HDC-CH capsule (left) and HDC capsule (middle), together with their radiation drives (right).

the ideal case of spherical symmetry, i.e., one-dimensional (1D) implosion, as compared in Table I. As shown in Fig. 1, the two capsules have the same fuel configuration, but their ablator configurations are a little different. The HDC capsule contains three layers of HDC ablator, consisting of undoped HDC, 0.1% W doped HDC and undoped HDC, same as in a traditional design of HDC capsule. In contrast, the HDC-CH capsule also has three ablator layers with the same middle and innermost layers as the HDC capsule, but it uses CH as its outmost ablator layer. The density is 1.05 g/cm^3 for CH, 3.52 g/cm^3 for 0.1% W doped HDC, 3.48 g/cm^3 for HDC, 0.44 mg/cm^3 for DT gas, and 0.255 g/cm^3 for DT ice. For both capsules, the DT mass is 165 μg, and the total ablator mass is about 3.2 mg. From the radiation drives shown in Fig. 1, the foot temperature is about 110 eV for the HDC-CH capsule, while 130 eV for the HDC capsule, high enough to melt crystal structure of HDC. The foot shapes are tuned so that the strength of the first shock is the same in the two capsules. According to our design, the CH layer of the HDC-CH capsule is completely ablated during the shock transit phase. Notice that the foot of HDC-CH design is about 2 ns longer than in HDC design, needing only about 18 kJ more, about 1% output of a laser facility of 1.8 MJ, inside an octahedral spherical hohlraum [22]with a hohlraum-to-capsule radius ratio of 5.

TABLE I. Comparisons of 1D implosion performances between HDC-CH and HDC capsules. All metrics except yield Y_{id} are calculated without alpha-particle energy deposition. The inflight fuel adiabat α_{if} is defined as ratio of shell pressure to Fermi-degenerate pressure calculated at the shell density at time of peak velocity.

Capsule	HDC-CH	HDC
Implosion velocity (km/s)	395	417
Adiabat α_{if}	2.32	2.37
$(\rho R)_{\text{fuel}}$ (g/cm^2)	1.14	1.11
Peak density ρ (g/cm^3)	554	541
Absorbed energy E_{cap} (kJ)	196	190
Ablator mass remaining (%)	7.7	5.2
Yield Y_{id} (MJ)	10	9.5

Simulations are used to compare the 1D implosion performances and 2D hydrodynamic instabilities between the two capsules with code LARED-S, a capsule-only radiation hydrodynamic code [23,24] widely used in ICF studies [25–27]. Presented in Fig. 2 is the Lagrangian shock plots for both capsules from 1D simulations of LARED-S. As shown, it has three shocks transiting the DT fuel layer and breaking out into the DT gas. The shock transit phase ends and acceleration phase starts at the time when the third shock transits the HDC/DT interface, and hereafter perturbations on the HDC/DT interface will not change phase. We denote the time when the third shock transits the HDC/DT interface as t_{DT}, which is about 6.8 ns for the HDC-CH capsule and 4.8 ns for the HDC capsule, respectively. According to our design of the HDC-CH capsule, the ablation front is inside the CH layer during whole shock transit phase.

As shown in Fig. 2, the shock series of the HDC-CH capsule during the shock transit phase seem more complex than the HDC capsule, because of the CH/HDC interface of the HDC-CH capsule. In the HDC-CH capsule, following the first shock breakout at the HDC/CH interface, the large density difference between CH and HDC simultaneously reflects a notable shock toward the ablation front. The first reflected shock first meets the second shock in CH, and then meets the ablation front. The merging of the first reflected shock with the ablation front again launches an inward shock which further merges with the second shock in DT ice fuel and finally coalesces with the first shock near the DT ice-gas interface. According to our design and

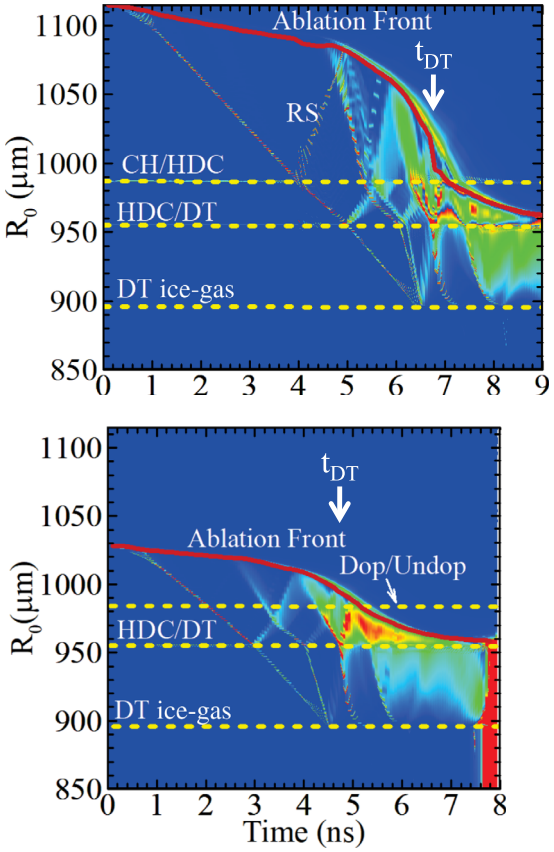

FIG. 2. Plots of the logarithmic radial derivative of hydrodynamic pressure in Lagrangian coordinate vs time space for HDC-CH capsule (upper) and HDC capsule (lower). The yellow dashed lines mark the locations of interfaces of DT ice-gas, HDC/DT and HDC/CH (or doped-undoped in HDC capsule), respectively, and the red lines denote the trajectory of ablation front. The time place of t_{DT} is marked by the white arrow lines.

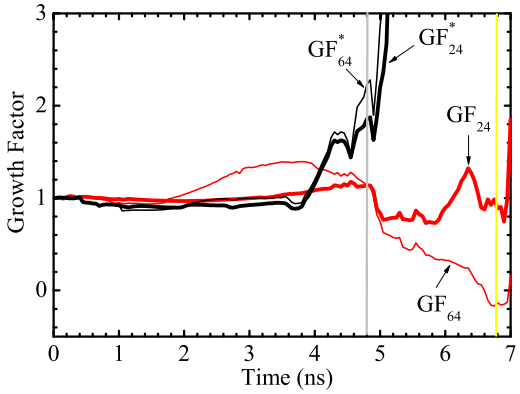

FIG. 3. Comparisons of temporal evolution of the ablation front linear growth factor during shock transit phase between the HDC-CH capsule (red) and the HDC capsule (black) for modes $L = 24$ (thick line) and $L = 64$ (thin line). The yellow and gray lines denote the place of t_{DT} in HDC-CH capsule and HDC capsule, respectively.

simulations on the HDC-CH capsule, its ablation front enters into HDC ablator shortly after t_{DT} and then the HDC/CH interface begins to expand outward. Thus, the CH layer has negligible effect on development of hydrodynamic instability in the following acceleration phase. For the HDC capsule, different from the HDC-CH capsule, it is the rarefaction reflected from the HDC/DT interface that the ablation front first meets during the shock transit phase.

We further use 2D simulations of LARED-S to compare HI of the two capsules by considering the single-mode surface perturbation in the form $\delta R = A_0 \cos(L\theta)$ initiated on the ablator outer surface. Here, $A_0 = 0.2$ μm is the initial perturbation amplitude. The simulations run on wedges with θ from $\pi/2 - \pi/L$ to $\pi/2 + \pi/L$ in a wide range of mode L. Shown in Fig. 3 is a comparison of evolutions of the ablation front linear growth factor (GF) of the two capsules during the shock transit phase, which is defined as the amplitude ratio at a fixed time to its initial value. For simplicity, we only present two characteristic modes, a lower mode $L = 24$ and a higher mode $L = 64$. In the following text, we use GF_{24} and GF_{64} to express ablation front GF of $L = 24$ and $L = 64$ of the HDC-CH capsule, and GF^*_{24} and GF^*_{64} to express those of the HDC capsule, respectively.

As shown in Fig. 3, the evolution of GF_{24}, GF^*_{24}, and GF^*_{64} is similar and keeps almost invariant around 1 till to the merging of the ablation front with the first reflected wave at about 3.8 ns for the HDC capsule and 4.8 ns for the HDC-CH capsule. The oscillation of GF_{64} is due to the higher ablation velocity and higher-frequency Richtmyer-Meshkov [28,29] oscillation in CH compared to HDC, which is important only at shorter wavelengths. However, the evolution is very different after the merging. In the HDC capsule, after the merging of ablation front with the first rarefaction wave reflected off HDC/DT interface, both GF^*_{24} and GF^*_{64} increase rapidly, and up to about 2 at t_{DT} when the shock transit phase ends. In contrast, for the HDC-CH capsule, the merging of the ablation front with the first shock reflected from the HDC/CH interface leads to the reductions of the amplitudes of GF_{24} and GF_{64}. As discussed below, the type of a reflected wave that reaches the ablation front first is responsible for this difference.

In the HDC design, a reflected rarefaction is formed when shock passes through HDC/DT interface. This rarefaction travels toward the ablation front and after its head reaches it, a pressure gradient is established which accelerates the ablation front for a short period of time and launches a compression wave back into the ablator [30]. During a short period of acceleration, the ablation front nonuniformity is amplified by the Rayleigh-Taylor (RT) growth (note that this happens prior to shell acceleration). This scenario is consistent with Fig. 3 where both GF^*_{24} and GF^*_{64} are amplified for a short time after the reflected rarefaction reaches the ablation front at 3.8 ns. In the case of HDC-CH target, a reflected shock is formed when the first

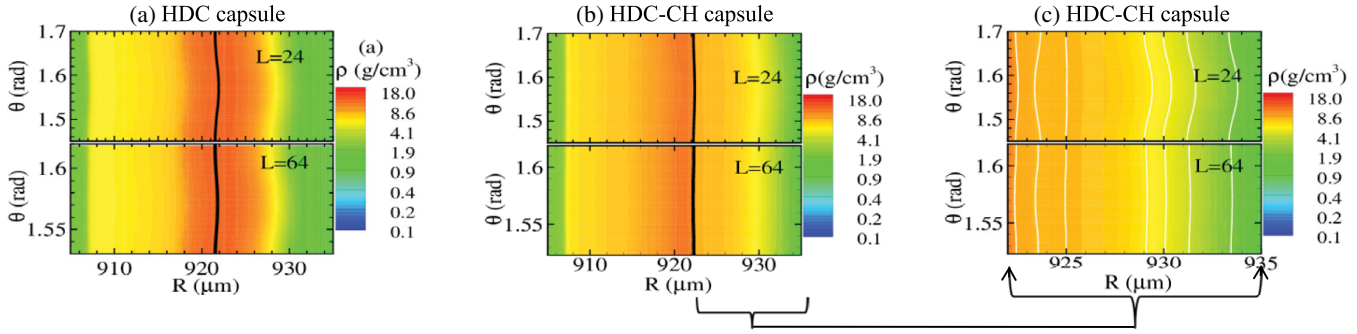

FIG. 4. Density contours for modes $L = 24$ and $L = 64$ in Lagrangian coordinate vs angle space of HDC capsule (a) and HDC-CH capsule [(b) and (c)] at a short time before t_{DT}. Notice that (c) presents the range of 922 to 935 μm of (b). The black line in (a) denotes the doped-undoped interface of HDC capsule and in (b) denotes the position of HDC/CH interface of HDC-CH capsule. The white lines in (c) are the density contours to show the negative perturbations of HDC-CH capsule, and the range between 922 and 925 μm is the inverse-phase region of HDC-CH capsule at this time.

shock passes the CH/HDC interface. When the reflected shock reaches the ablation front, the latter experiences deceleration (as opposite to acceleration in the HDC case). Decelerated ablation front is RT stable and perturbations start to oscillate, similar to water waves in gravitational field. The reflected rarefaction from HDC/DT interface is also formed in this design. It reaches the ablation front at 6 ns. At that time the amplitude experiences a short RT growth but it starts with much smaller amplitude which was reduced by deceleration from the reflected shock.

It is interesting that the reflected shock from the HDC/CH interface generates an inverse-phase region between and the ablation front for the HDC-CH capsule. Shown in Fig. 4 is a visual comparison of the density contours between the HDC-CH capsule and the HDC capsule at a short time before t_{DT}. As shown, the ablation front of the HDC-CH capsule locates at about 930 μm, ~8 μm away from the HDC/CH interface; and for the HDC capsule, it locates at about 927 μm, ~5 μm away from the doped-undoped interface. From Fig. 4(a), the perturbation phase of the HDC capsule keeps the same in whole region between the ablation front and the doped-undoped interface. However, for the HDC-CH capsule, it exists an inverse-phase region in the CH layer, where the perturbation phase is opposite to that on ablation front, as shown in Figs. 4(b) and 4(c).

We further compare the linear GF spectra at the ablation front and at the fuel-ablator (DT/HDC) interface between the two capsules at t_{DT} in Fig. 5(a) and at the implosion velocity peak in Fig. 5(b). As shown in Fig. 5(a), the amplitudes of two interfaces in HDC-CH capsule are significantly smaller than the respective interfaces in HDC capsule. For HDC capsule, the ablation front GF spectra is all positive, with the peak GF of 2.3 locating at $L = 64$ and the zero point locating at mode larger than $L = 200$. In contrast, for HDC-CH capsule, the ablation front GF peaks at a smaller mode of $L = 24$ with an obvious smaller peak value of about 0.9. Especially, the ablation front GF spectra of HDC-CH capsule has two zero points at $L \sim 48$ and $L \sim 180$, and GF at modes larger than $L = 48$ is all close to zero. It worth to mention that, for the mode $L = 64$ which has the largest growth during the acceleration phase of the HDC capsule, its GF is only ~ -0.2, reduced by $\sim$ one order of absolute magnitude, in the HDC-CH capsule design. Again, from Fig. 5(b), the

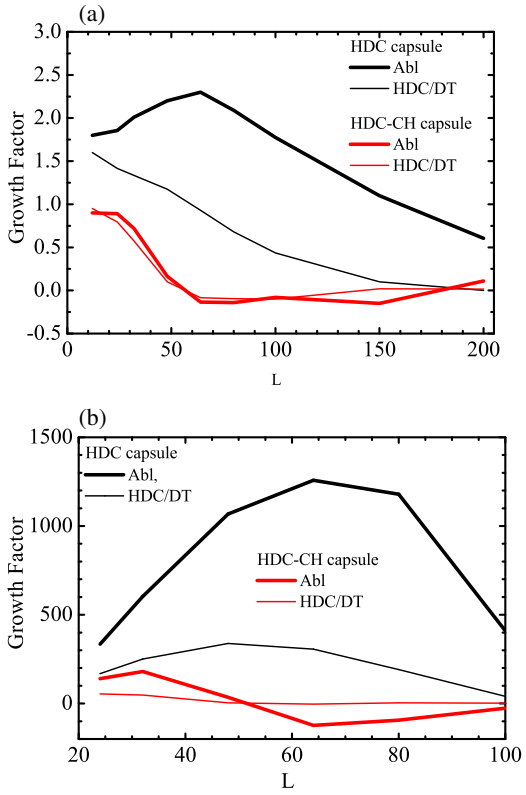

FIG. 5. Comparisons of ablation front linear GF (thick lines) and DT/HDC interface linear GF (thin lines) between HDC capsule (black lines) and HDC-CH capsule (red lines) at t_{DT} (a) and at peak implosion velocity (b), with perturbations initially seeded on the ablator outer surface.

linear GF spectra at the peak implosion velocity of the HDC-CH capsule are remarkably smaller than the respective interfaces in HDC capsule. As shown, the HDC capsule has much larger and positive GF spectra, with a peak of 1250 at $L = 64$. In contrast, the HDC-CH capsule shows significantly reduced GF with a much lower GF peak of 180 at $L = 32$, reduced by about 7 times as compared to the peak GF of the HDC capsule. As shown, GF at $L = 64$ is only 124 for the HDC-CH capsule, reduced by $\sim$ one order of magnitude as compared to GF at $L = 64$ of the HDC capsule.

In summary, for the first time the use of two different ablators in indirect-drive central hot spot ignition capsule design is proposed. Our 2D simulation studies convincingly demonstrate that the additional reflected shock from the HDC/CH interface of the HDC-CH capsule can significantly reduce the ablation front growth factor at both the end of shock transit phase and the time at peak implosion velocity. Small surface roughness at the HDC/CH interface may be required for the novel design, which can influence the ablation front via the first reflected shock from this interface. By keeping HDC as the main ablator for maintaining its advantage of short laser pulses for a low level of LPI and a better symmetry control, this novel HDC-CH capsule design has the advantages of low HI and low LPI, which provides a larger margin toward ICF ignition.

The authors would like to thank Professor Z. Feng, Professor W. H. Ye, and Dr. Y. S. Li of IAPCM and Professor Vladimir Tikhonchuk of ELI-Beamlines for beneficial discussions on implosion physics, and thank Professor Bo Li of IFRC for beneficial discussions on target fabrications. In particular, we acknowledge all referees of our Letter, especially the generous and valuable help from referee B on understanding the hydrodynamic instability of our novel design. This work is supported by the National Natural Science Foundation of China (Grant No. 12035002).

*lan_ke@iapcm.ac.cn

[1] J. Nuckolls, L. Wood, A. Thiessen, and G. Zimmermann, Nature (London) **239**, 139 (1972).
[2] S. Atzeni and J. Meyer-ter-vehn, *The Physics of Inertial Fusion* (Clarendon, Oxford, 2004).
[3] R. Betti and O. A. Hurricane, Nat. Phys. **12**, 435 (2016).
[4] J. D. Lindl, Phys. Plasmas **2**, 3933 (1995).
[5] G. H. Miller, E. I. Moses, and C. R. Wuest, Opt. Eng. **43**, 2841 (2004).
[6] E. M. Campbell *et al.*, Matter Radiat. Extremes **2**, 37 (2017).
[7] O. A. Hurricane *et al.*, Nature (London) **506**, 343 (2014).
[8] O. A. Hurricane *et al.*, Nat. Phys. **12**, 800 (2016).
[9] S. Le Pape, L. F. Berzak Hopkins, L. Divol, A. Pak, E. L. Dewald *et al.*, Phys. Rev. Lett. **120**, 245003 (2018).
[10] A. B. Zylstra, A. L. Kritcher, O. A. Hurricane, D. A. Callahan, K. Baker *et al.*, Phys. Rev. Lett. **126**, 025001 (2021).
[11] R. E. Olson, G. A. Rochau, O. L. Landen, and R. J. Leeper, Phys. Plasmas **18**, 032706 (2011).
[12] J. L. Kline and J. D. Hager, Matter Radiat. Extremes **2**, 16 (2017).
[13] T. Döppner *et al.*, Phys. Plasmas **27**, 042701 (2020).
[14] S. W. Haan *et al.*, Phys. Plasmas **18**, 051001 (2011).
[15] J. Nilsen *et al.*, Matter Radiat. Extremes **5**, 018401 (2020).
[16] L. F. B. Hopkins *et al.*, Phys. Rev. Lett. **114**, 175001 (2015).
[17] D. Turnbull *et al.*, Phys. Plasmas **23**, 052710 (2016).
[18] J. L. Kline *et al.*, Nucl. Fusion **59**, 112018 (2019).
[19] D. S. Clark, A. L. Kritcher, S. A. Yi, A. B. Zylstra, S. W. Haan, and C. R. Weber, Phys. Plasmas **25**, 032703 (2018).
[20] A. L. Kritcher *et al.*, Phys. Plasmas **25**, 056309 (2018).
[21] A. Pak, L. Divol, C. R. Weber, L. F. Berzak Hopkins, D. S. Clark *et al.*, Phys. Rev. Lett. **124**, 145001 (2020).
[22] K. Lan, J. Liu, D. Lai, W. Zheng, and X.-T. He, Phys. Plasmas **21**, 010704 (2014); K. Lan, X.-T. He, J. Liu, W. Zheng, and D. Lai, Phys. Plasmas **21**, 052704 (2014); K. Lan and W. Zheng, Phys. Plasmas **21**, 090704 (2014); K. Lan *et al.*, Matter Radiat. Extremes **1**, 2 (2016).W. Y. Huo, Z. Li, Y. H. Chen, X. Xie, G. Ren *et al.*, Phys. Rev. Lett. **120**, 165001 (2018).
[23] W. Ye, W. Zhang, and X. T. He, Phys. Rev. E **65**, 057401 (2002).
[24] Z. Fan, Europhys. Lett. **99**, 65003 (2012).
[25] D. Yuan *et al.*, Astrophys. J. **815**, 46 (2015).
[26] L. F. Wang *et al.*, Phys. Plasmas **23**, 052713 (2016).
[27] X. Qiao and K. Lan, Plasma Phys. Controlled Fusion **61**, 014006 (2019).
[28] R. D. Richtmyer, Commun. Pure Appl. Math. **13**, 297 (1960).
[29] V. N. Goncharov *et al.*, Phys. Plasmas **13**, 012702 (2006).
[30] V. N. Goncharov, S. Skupsky, T. R. Boehly, J. P. Knauer, P. McKenty, V. A. Smalyuk, R. P. J. Town, O. V. Gotchev, R. Betti, and D. D. Meyerhofer, Phys. Plasmas **7**, 2062 (2000).